Heavy-ion effects: from track structure to DNA and chromosome damage

New Journal of Physics
The open-access journal for physics

Heavy-ion effects: from track structure to DNA and chromosome damage

F Ballarini[1,2], D Alloni[1,3], A Facoetti[1,2] and A Ottolenghi[1,2,4]

[1] Department of Nuclear and Theoretical Physics, University of Pavia, via Bassi 6, I-27100 Pavia, Italy
[2] INFN (National Institute of Nuclear Physics), Sezione di Pavia, via Bassi 6, I-27100 Pavia, Italy
[3] LENA (Laboratory of Applied Nuclear Energy), University of Pavia, via Aselli 41, I-27100 Pavia, Italy
E-mail: francesca.ballarini@pv.infn.it and andrea.ottolenghi@pv.infn.it

New Journal of Physics **10** (2008) 075008 (17pp)
Received 1 February 2008
Published 28 July 2008
Online at http://www.njp.org/
doi:10.1088/1367-2630/10/7/075008

Abstract. The use of carbon ions for the treatment of certain tumour types, especially radioresistant tumours, is becoming more frequent due to the carbon-ion dose localization and high relative biological effectiveness (RBE) in the Bragg peak region. Human beings can also be exposed to heavy ions in space, since galactic cosmic rays are a mixed field consisting of not only high-energy protons and He ions, but also heavier ions including iron. Due to their high linear energy transfer (LET), heavy ions have peculiar track structures, characterized by a high level of energy deposition clustering. Furthermore, high-energy ions produce energetic secondary electrons ('delta rays') which can give rise to energy depositions several micrometres away from the core of the primary particle track. Also in view of hadron therapy and space radiation applications, it is therefore important to characterize heavy-ion tracks from a physical and biophysical point of view. In this framework, herein we will discuss the main physical features of heavy-ion track structure, as well as heavy-ion-induced DNA double-strand breaks, which are regarded as one of the most important initial radiobiological lesions and chromosome aberrations, which are correlated both with cell death and with cell conversion to malignancy.

[4] Author to whom any correspondence should be addressed.

Contents

1. Introduction

Carbon ions are now used in an increasing number of cancer therapy centres including Chiba (with about 3800 patients treated since 1994) and Hyogo, in Japan (270 since 2002), and Darmstadt, in Germany (380 since 1997). New carbon facilities are under construction in Pavia (Italy), Heidelberg (Germany) and other locations (see Amaldi and Kraft 2007, for a review). Like protons, carbon ions are characterized by a localization of energy deposition at the depth of penetration in the so-called 'Bragg peak' region. This can provide an improved dose conformation with respect to photons, also considering that the relative biological effectiveness (RBE) of therapeutic carbon ions in the plateau before the peak is sufficiently low. Furthermore, carbon beams are particularly suitable for treating radioresistant tumours because their RBE in the region of the spread-out Bragg peak (SOBP) can be up to 3 (also depending on the beam features, the considered cell line, etc). However, treatment planning with carbon ions is particularly complex also considering that, at the energies of interest for hadron therapy, nuclear reactions of the primary particles with the beam-line constituents and with the various components of the human body can modify the radiation field giving rise to projectile and target fragments.

The exposure to space radiation represents another situation where human beings can be irradiated by heavy ions. The scenario is made particularly complex by the fact that galactic cosmic rays (GCR) are a mixed field consisting of high-energy protons (about 87% in fluence), He ions (12%) and heavier ions (1%), the latter also called 'HZE particles' (high atomic number 'Z' and energy 'E'). Astronauts are exposed to GCR continuously, with a dose rate of the order of 1 mSv day^{-1} in deep space. Despite their small contribution to the fluence, the contribution of heavy ions to the total equivalent dose can be much higher, up to 50% (Durante 1996). Due to the complexity of the exposure scenario and to the fact that some aspects of heavy-ion radiobiology are still not clear, the physical dose is not sufficient to estimate the corresponding damage and risk. Similarly to what happens for carbon therapy (see below), biological dosimetry with chromosome aberrations (CAs) can be helpful. Indeed, monitoring of CAs in astronauts' peripheral blood lymphocytes (PBL) has become routine in the last decade; more details will be provided in section 4.2.

Heavy ions have a peculiar track structure characterized by high levels of energy-deposition clustering. (The expression 'track structure' refers to an 'event-by-event' description of the physical processes following irradiation, represented as a matrix $S_n(i, \boldsymbol{X}, E)$, where i is the interaction type, $\boldsymbol{X}$ is its position, and E is the deposited energy.) Furthermore, energetic ions can produce high-energy secondary electrons which can give rise to energy depositions several micrometres away from the primary particle. Also in view of hadron therapy and space radiation applications, the physical and biophysical characterization of heavy-ion tracks is therefore of utmost importance.

In this framework, in section 2, we will discuss the main physical features of heavy-ion track structure (including inelastic scattering cross-sections in liquid water), which has significant consequences on radiobiological damage at different levels. In the following, we will focus on DNA damage and chromosome damage, since: (i) DNA double-strand breaks (DSBs) are regarded as one of the most important initial radiobiological lesions (though also the so-called 'non-targeted effects', such as the bystander effect, can play a significant role); (ii) CAs are a particularly relevant endpoint due to their correlation both with cell death, with possible applications in radiotherapy, and with cell conversion to malignancy, with possible applications for evaluating radiation protection. More specifically, in section 3, we will analyse heavy-ion-induced DNA DSBs with a focus on the role of spatial correlations of the DSBs within the DNA molecule, and between specific chromosomes within the nucleus, whereas in section 4, we will discuss heavy-ion-induced CAs again with focus on the role of DSB clustering, as well as peculiar features of heavy ions such as the induction of complex exchanges (i.e. those aberrations involving at least 3 breaks and 2 chromosomes) and of interphase death/mitotic delay.

2. Heavy-ion track structure

It is well known that the features of radiation track structure at the nanometre level have important implications in terms of radiation effects in biological targets. This is especially true for energetic ions, which have complex track structures characterized by energy depositions not only along the primary-particle path, but also projected out radially with respect to the track 'core'. This is due to the so-called 'delta rays', i.e. high-energy secondary electrons which can travel distances of the order of tens of micrometres in biological targets. The effects of heavy ions, especially for high-energy primary ions, are further complicated by nuclear interactions, which can give rise to both projectile and target fragments including neutrons. On this subject, it is worth mentioning that while in nuclear physics, carbon ions are generally classified as 'light ions', in radiobiology and hadron therapy ions heavier than He—thus including carbon—are generally referred to as 'heavy'. A detailed discussion on heavy-ion-induced nuclear interactions is beyond the scope of the present paper. However, it is worth mentioning that projectile fragments have a high probability to proceed with the same direction and velocity as the primary particle, whereas target fragments (including carbon, oxygen and lighter particles such as protons and helium ions) generally have lower velocity—and thus higher LET—and can be significantly scattered with respect to the primary-ion trajectory.

Models and codes based on the Monte Carlo techniques represent very good tools to simulate 'event-by-event' radiation track structure at the nanometre level, taking into account each single energy-deposition event. In view of radiobiology applications, most of these codes are based on cross sections in liquid water, which is considered to be a good surrogate for

biological targets. Older codes, based on water-vapour cross sections, are now considered obsolete because of the significant differences between liquid and vapour phase water. Although heavy-ion cross sections in liquid water are known with less detail with respect to light-ions, significant advances have been achieved in the last few years.

2.1. Inelastic scattering cross sections in liquid water

Energy deposition by charged particles mainly occurs via the Coulomb-field interaction, and the formal theoretical description of this kind of interaction is well developed. The numerical evaluation of cross sections is very difficult in condensed media, where one deals with many-body systems containing a large number of targets. In contrast to the gas-phase, where isolated molecules or atoms have to be taken into account, for condensed matter it is not possible to obtain with sufficient accuracy the target wave functions and the *eigenvalues* with methods such as the Hartree–Fock techniques. The main phase-specific difference between condensed and gas-phase matter is that condensed matter is characterized by collective (coherent) excitations induced by the charged-particle passage. These quanta are delocalized and cover a macroscopic spatial region, and then decay by single-particle excitations.

For energy values below the relativistic threshold, such inelastic processes are well described by the non-relativistic first Born approximation (NR-FBA) coupled with the dielectric theory (DT). While the NR-FBA is a perturbative treatment valid only for projectiles that are sufficiently fast but still in the non-relativistic regime, the latter is adopted to describe the condensed medium collective response to external perturbations that is the charged-particle passage.

Using the quantum mechanical approach, it is possible to obtain the general expression of the differential cross section in the solid angle $\mathrm{d}\Omega = \sin\theta\,\mathrm{d}\theta\,\mathrm{d}\varphi$ (θ is the angle between the initial and final particle momenta $\mathbf{k}$ and $\mathbf{q}$) for the transition of the projectile (plus target) system from the initial state $|i\rangle = |\mathbf{q}, E_\mathrm{i}\rangle$ to the final state $|f\rangle = |\mathbf{k}, E_\mathrm{f}\rangle$

$$\frac{\mathrm{d}\sigma_{\mathrm{i}\to\mathrm{f}}}{\mathrm{d}\Omega} = \frac{k}{q}\left|\frac{2m}{4\pi}\langle\mathbf{k}, E_\mathrm{f}|V|\mathbf{q}, E_\mathrm{i}\rangle\right|^2, \tag{1}$$

where V is the interaction potential between the projectile and the target, m is the mass of the projectile and E_i and E_f refer to the initial and final energy configurations of the target. The quantity $\sigma_{\mathrm{i}\to\mathrm{f}}$ is the total cross section that can be obtained after integration of equation (1) over the entire range of angular variables. Energy conservation allows only particles with energy $\omega = E_\mathrm{f} - E_\mathrm{i}$ to emerge from the collision process. The double-differential cross section into the solid angle and for energy transfer $\mathrm{d}\omega$ can then be written as

$$\frac{\mathrm{d}^2\sigma_{\mathrm{i}\to\mathrm{f}}}{\mathrm{d}\Omega\,\mathrm{d}\omega} = (2\pi)^6\frac{k}{q}\left|\frac{2m}{4\pi}\langle\mathbf{k}, E_\mathrm{f}|V|\mathbf{q}, E_\mathrm{i}\rangle\right|^2\delta\left(\omega + E_\mathrm{i} - E_\mathrm{f}\right), \tag{2}$$

where the Dirac delta-function ensures energy conservation. Assuming that the potential V depends only upon the coordinates of the projectile $\mathbf{r}$ and of targets (atomic electrons) $\mathbf{r}_\mathrm{j}$ (like in the case of the Coulomb potential, once the charges involved are known), equation (2) can be further simplified leading to an expression rewritten in terms of energy ω and transferred momentum $\mathbf{p} = \mathbf{q} - \mathbf{k}$

$$\frac{\mathrm{d}^2\sigma\,(\mathbf{p}, \omega)}{\mathrm{d}p\,\mathrm{d}\omega} = \frac{2\pi p}{q}\left|V(\mathbf{p})\right|^2 S\,(\mathbf{p}, \omega), \tag{3}$$

where the term $S(\mathbf{p}, \omega)$ is by definition the dynamic form factor (DDF) (Landau *et al* 1984, Pines and Nozieres 1966).

In principle, this expression contains all the information needed for the calculation of scattering probabilities, and is given as a product of two factors: $|V(\mathbf{p})|^2$ contains information on the projectile–target interaction, whereas the DDF describes the target.

Expression (3) can be provided in a form which is more convenient for the calculations. This is obtained replacing the DDF with the dielectric response function (DRF) $\varepsilon(\mathbf{p},\omega)$ of the system (the medium), allowing for an easier interpretation. The DRF is defined in terms of the electric field $\mathbf{E}$ and the dielectric displacement $\mathbf{D}$ induced by a charged projectile of charge density $\rho_{\mathrm{P}}(\mathbf{r}, \mathrm{t})$

$$E(\mathbf{p}, \omega) = D(\mathbf{p}, \omega)/\varepsilon(\mathbf{p}, \omega).$$

From the Maxwell equations, it is possible to obtain an expression for $1/\varepsilon(\mathbf{p},\omega)$ in terms of the projectile charge density and of the target charge-density fluctuation induced by the projectile itself

$$\frac{1}{\varepsilon(\mathbf{p}, \omega)} = 1 + \frac{\langle \Delta\rho_{\mathrm{T}}(\mathbf{p}, \omega)\rangle}{\rho_{\mathrm{P}}(\mathbf{p}, \omega)}.$$

To calculate $1/\varepsilon(\mathbf{p}, \omega)$, we need to obtain an expression for the ratio containing the densities. The general lines to obtain the ratio consider the medium linear response to projectile perturbation, where 'linear' response means for sufficiently weak perturbations described by the interaction potential representing the Coulomb interaction between the two charge densities. To evaluate the system (medium) charge-density fluctuation under the influence of the projectile, the target wave function is also needed. This is achieved starting from the Schrödinger equation describing the target subject to the interaction potential and solving the problem by Green's functions techniques. The final expression obtained for $1/\varepsilon(\mathbf{p},\omega)$ (which contains the target *eigenvectors*) allows one to express its imaginary part in terms of the DDF

$$\mathrm{Im}\left\{\frac{1}{\varepsilon(\mathbf{p}, \omega)}\right\} = \frac{4\pi}{p^2}\left[S(\mathbf{p}, -\omega) - S(\mathbf{p}, \omega)\right].$$

Besides these calculations, we are interested in the final expression of the double-differential cross section (in energy and momentum transfers) for positive energy transfers ($\omega > 0$)

$$\frac{\mathrm{d}^2\sigma}{\mathrm{d}\mathbf{p}\,\mathrm{d}\omega} = \frac{2}{q^2}\frac{1}{p}\mathrm{Im}\left\{-\frac{1}{\varepsilon(\mathbf{p}, \omega)}\right\}. \tag{4}$$

Here, q is the projectile initial momentum, whereas $\mathbf{p}$ and ω are the transferred momentum and energy, respectively. For a particle of charge Z and velocity v, we can rewrite equation (4) in the more familiar form of double-differential cross section per atomic electron

$$\frac{\mathrm{d}^2\sigma(\mathbf{p}, \omega)}{\mathrm{d}\mathbf{p}\mathrm{d}\omega} = \frac{2Z^2e^2}{\pi N\hbar v^2}\frac{1}{p}\mathrm{Im}\left\{-\frac{1}{\varepsilon(\mathbf{p}, \omega)}\right\}. \tag{5}$$

The calculation of $\varepsilon(\mathbf{p},\omega)$ is beyond the current computational capabilities, since it requires a quantum mechanical description of the system band structure and its wave functions, and atomic hydrogen is the only system for which $\varepsilon(\mathbf{p},\omega)$ is exactly known. A number of different approaches (Dingfelder *et al* 1998, 2000, Ehrenreich and Cohen 1959, Heidin and Lundqvist 1969, Ritchie *et al* 1988, Zaider *et al* 1990) have been proposed for the modellization of $\varepsilon(\mathbf{p},\omega)$. Such approaches are based on the experimental optical data $\varepsilon(\mathbf{p} = 0,\omega)$

and are focused on the extrapolation of the expression of $\varepsilon(\mathbf{p},\omega)$ to nonzero momentum transfer ($\mathbf{p} \neq 0$) (the Bethe surface) and to large momentum transfer (the Bethe ridge).

An example of Monte Carlo code based on radiation track structure in liquid water is provided by PARTRAC, a biophysical code mainly developed at GSF (Munich, Germany) able to simulate DNA damage in human cells based on the superposition of simulated track structures to an 'atom-by-atom' model of human DNA, also taking into account the higher-order DNA organization in terms of chromatin fibre and chromosome territories (e.g. Friedland *et al* 2008).

In the initial version of the PARTRAC code, it was possible to perform irradiation simulations only with photons, electrons, protons and alpha particles. Recently, the code physical module has been suitably modified to adapt the code to reproduce the physics (i.e. the track structure) of basically any type of primary ion in the non-relativistic regime. As an example, taking into account the Z^2 dependence of equation (5) (valid for protons and electrons), the mean free path (MFP) λ_{ion} of the primary ion was obtained rescaling the proton MFP

$$\lambda_{\text{ion}} = \lambda_{\text{proton}} \cdot \frac{1}{\left(Z^*_{\text{ion}}\right)^2},$$

where Z^* is the ion effective charge, which takes into account charge-exchange processes via the Barkas formula

$$Z^*_{\text{ion}} = Z_{\text{ion}}\left[1 - \exp(-125\beta/Z^{2/3})\right].$$

A first validation of the correctness of the adopted method was obtained by preliminary tests reproducing radial distributions of energy and dose following irradiation with different ions of interest for basic radiobiology, hadron therapy and radiation protection, including heavy ions (Alloni 2008, Liotta 2005). Figure 1 shows two-dimensional (2D) projections of sample tracks of H-, He-, C- and Fe-ions with the same energy per nucleon (115 MeV n^{-1}), and thus the same velocity, as calculated with the PARTRAC code in liquid water. As expected, heavy-ion track structures are more 'dense' with respect to light ions with the same velocity, due to the fact that the LET is directly proportional to the square of the particle (effective) charge. These results are consistent with the earlier work by Chatterjee and Schaefer (1976).

Figure 2 shows 3D track-structure segments in liquid water for iron ions with different energies (115 and 414 MeV u^{-1}, with the corresponding LET values of 442 and 201 keV micron^{-1}, respectively) as calculated with PARTRAC. Increasing the ion energy (per nucleon), and thus the velocity, the tracks become less clustered due to the lower LET, but their delta rays are more energetic and thus can travel further away from the primary-ion track core. This can have important consequences in terms of radiobiological damage, because energetic delta rays can reach the neighbouring cells.

3. Heavy ions and DNA damage

It is widely accepted that DNA DSBs are critical lesions in the pathways leading from the initial energy deposition by radiation to radiobiological damage at sub-cellular and cellular levels, including gene mutations, CAs, neoplastic transformation and clonogenic inactivation. The spatial distribution of the initial DSB plays a key role in determining the fate of irradiated cells, since the sub-cellular and cellular endpoints mentioned above depend on the features of the DSB ensemble induced by the irradiation (Goodhead 1994). The spatial correlation of DSB,

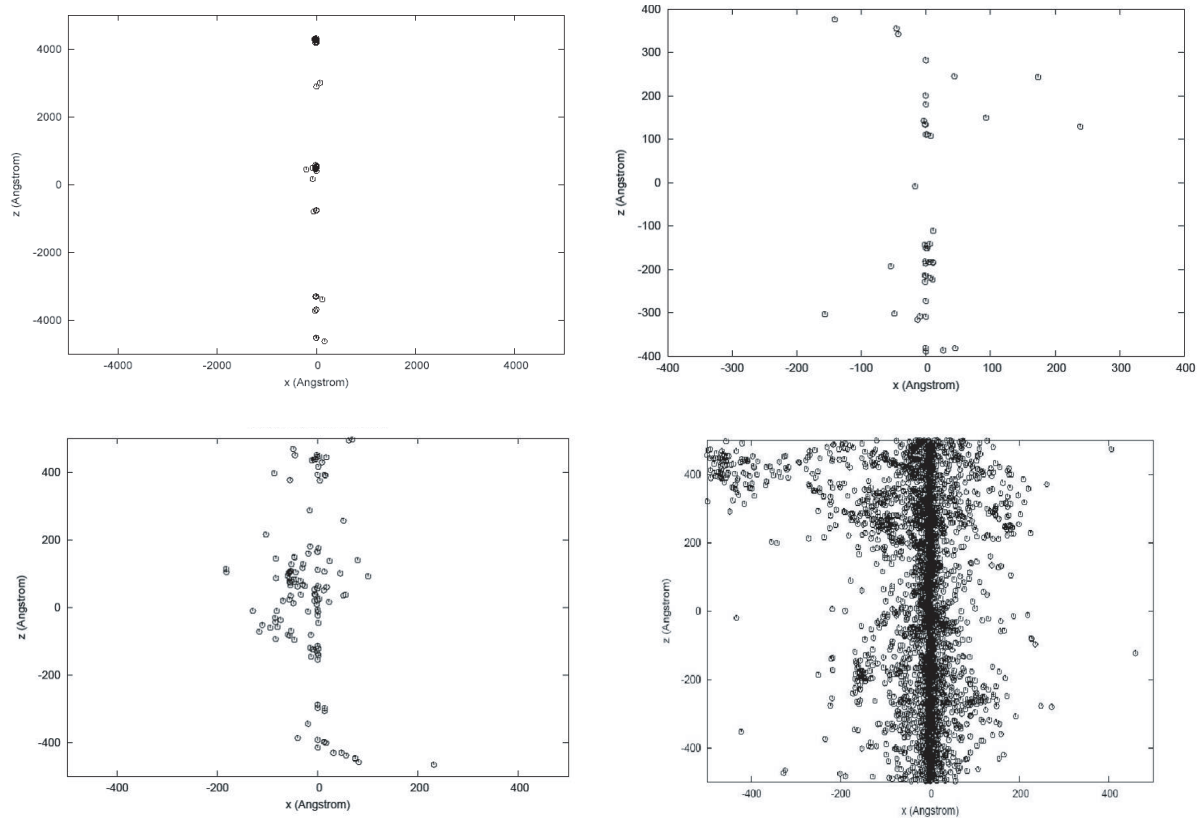

Figure 1. 2D projection of track-structure segments in liquid water for different ions with the same velocity (115 MeV nucleon^{-1}) as calculated with the PARTRAC code (from top to bottom and from left to right: H, He, C and Fe; note the different scale for the proton track).

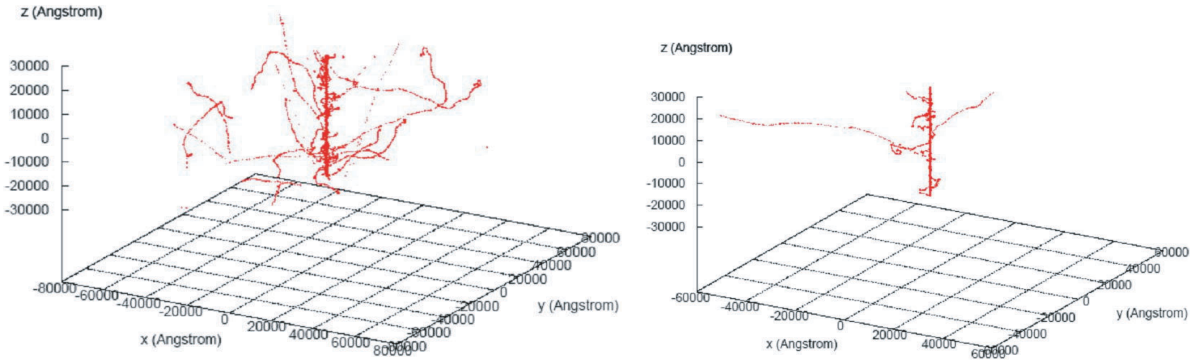

Figure 2. 3D representations of track-structure segments in liquid water for iron ions with different energies as calculated with the PARTRAC code. Left panel: 115 MeV u^{-1} Fe ion; right panel: 414 MeV u^{-1} Fe ion. The corresponding LET values are 442 keV micron^{-1} and 201 keV micron^{-1}, respectively.

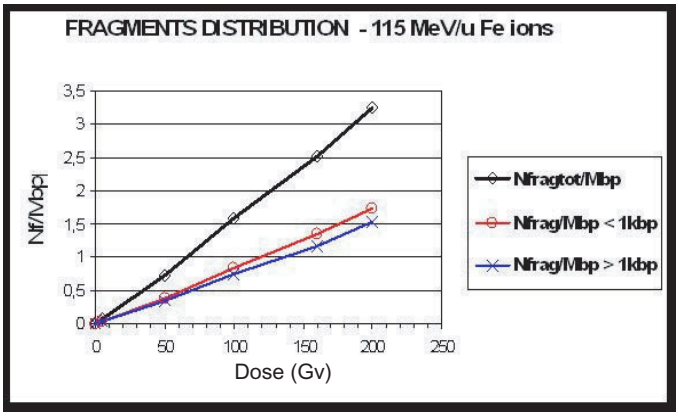

Figure 3. Yields of DNA fragments (per Mbp) of different sizes (O *symbols, fitted by red line: smaller than 1 kbp;* × *symbols, fitted by blue line: larger than 1 kbp;* ◊ *symbols, fitted by black line: any size*) induced by 115 MeV u^{-1} Fe ions as calculated with the PARTRAC code for the following dose values: 5, 50, 100, 150 and 200 Gy. Simulation error bars are smaller than the symbol sizes.

both in terms of geometrical distance and in terms of 'genomic distance' (i.e. in base-pairs), is thought to influence the DSB reparability. This implies that the radiobiological effects induced by a given radiation dose depend on the radiation quality, since the DSB distribution will be determined not only by chromatin conformation, but also by radiation track-structure at the nanometre level. Experimental and theoretical studies (Holley and Chatterjee 1996, Friedland *et al* 1998, 2003, Rydberg 1996, Rydberg *et al* 1998) outlined the existing correlation of radiation-induced DSB at the nucleosome scale (that is 100 base-pairs or bp), and at the low-level chromatin fibre organization scale (that is 1 kbp). For high-LET radiation, including heavy ions, such a correlation is much higher than for low-LET radiation. Even at larger scales, where the distribution of the DSB induced by low-LET radiation is basically random, high-LET radiation can produce a DSB distribution that deviates significantly from randomness (Belli *et al* 2002, Frankenberg *et al* 1999, Höglund *et al* 2000, Löbrich *et al* 1996, Newman *et al* 1997, Campa *et al* 2004, 2005). The statistical properties of the induced DSB can be investigated analysing the DNA fragment size distributions produced after irradiation. The analysis of DNA fragment spectra can provide important contributions with the aim of performing reliable predictions of the consequences of heavy-ion irradiation.

In the present paper, we report a theoretical analysis, performed by means of the PARTRAC code, of DNA fragment spectra induced by 115 MeV u^{-1} Fe ions (LET in water 442 keV $micron^{-1}$) in human fibroblasts (Alloni 2008, Alloni *et al* 2007). Figure 3 reports yields of DNA fragments (per Mbp) of different sizes (i.e. smaller than 1 kbp, larger than 1 kbp and of any size) induced by 115 MeV u^{-1} Fe ions as calculated with PARTRAC for the following dose values: 5, 50, 100, 150 and 200 Gy. Each point in figure 3 was obtained running the code 10 times for each considered dose value. This way, the error bars are smaller than the symbols themselves. The 1 kbp 'threshold' was chosen because fragments smaller than 1 kbp can hardly be detected with the currently available experimental techniques.

Qualitatively, the dose response is basically linear both for fragments smaller than 1 kbp and for larger fragments. Importantly, fragments smaller than 1 kbp account for about half of the total fragments (i.e. all sizes), leading to a higher RBE value with respect to the fragments of any size. This reflects the role of radiation track-structure, which for high-LET radiation—including heavy ions—is particularly effective at producing clustered energy depositions and thus very small DNA fragments.

Despite the fact that the experimental detection of such fragments is difficult, these fragments can play an important role in the evolution of the initial DNA damage in terms of subsequent endpoints at sub-cellular and cellular level, because clustered DNA breaks are more difficult to repair correctly and thus can give rise to gene mutations, CAs, etc. In this context, in the next section, we will discuss CA induction by heavy ions and will present a theoretical model based on the assumption that only clustered—and thus severe—DNA breaks can give rise to CAs.

4. Heavy ions and CAs

4.1. CA induction by heavy ions in vitro

Most information on CA induction by heavy ions comes from *in vitro* experiments where living cells, quite often lymphocytes or fibroblasts, are exposed to carbon ions, which are of interest for hadron therapy, or heavier ions such as iron, silicon and other ions that are of interest for space radiation research. Available literature data (e.g. Durante *et al* 1997, 1998, 1999, George *et al* 2001b, 2003, Kawata *et al* 2001, Ohara *et al* 1998, Testard *et al* 1997, Wu *et al* 1997) indicate that the linear coefficient for the induction of dicentric chromosomes increases with the radiation LET, peaking around 60–100 keV micron^{-1}, and decreases sharply at higher LET values.

Heavy ions are particularly effective at inducing complex exchanges. Since most complex exchanges cannot be scored with conventional Giemsa staining, with which all chromosomes appear in the same colour, the most recent studies employ the fluorescence *in situ* hybridization (FISH) technique, which allows selective 'painting' of specific chromosomes or even chromosome regions. The results of FISH experiments on CA induction by heavy ions indicate a much higher frequency of complex exchanges compared to low-LET radiation, and the observed rearrangements are of greater complexity. Another peculiarity of heavy ions, and more generally high-LET radiation, is given by their high effectiveness at inducing mitotic delay and interphase cell death. It is therefore desirable that the analysis of heavy-ion-induced CAs is performed by premature chromosome condensation (PCC), which allows CA scoring during interphase thus reducing the cell population selection bias in metaphase, leading to higher RBE values. Indeed the frequency of heavy-ion-induced CAs observed with PCC in interphase is significantly higher than the frequency observed in metaphase (Durante *et al* 1997, 1999, George *et al* 2001b, Goodwin *et al* 1994). Also crucial for heavy-ion-induced CAs is the timing of scoring, in order to account for significant mitotic delays. More details on this issue can be found in Ritter *et al* (2002), Nasonova and Ritter (2004) and Gudowska-Nowak *et al* (2005).

A very complete and informative study of CA induction by heavy ions was performed by George *et al* (2003), who irradiated *in vitro* human lymphocytes with several ions

including 290 MeV n^{-1} C-12 (LET in water = 13.3 keV micron^{-1}), 490 MeV n^{-1} Si-28 (LET = 56 keV micron^{-1}), 550 MeV nucleon^{-1} Ar-40 (LET = 86 keV micron^{-1}), 1040 MeV n^{-1}Fe-56 (LET = 147 keV micron^{-1}), 500 MeV n^{-1} Fe-56 (LET = 200 keV micron^{-1}), 200 MeV n^{-1} Fe-56 (LET = 440 keV micron^{-1}) and 10 000 MeV n^{-1} Au-197 (LET = 1393 keV micron^{-1}). (The reported energy values refer to the nominal energy of the extracted beam.) In most cases, the doses were lower than 1 Gy, and simple and complex exchanges were scored by whole-chromosome FISH painting. For carbon and iron, the analysis was performed not only at the first post-irradiation mitosis, but also earlier in interphase following chemically induced PCC after radiation exposure. For all the considered ions, PCC values were found to be higher than metaphase values by a factor ranging between 2 and 3. RBE values for metaphase simple exchanges (i.e. dicentrics plus reciprocal translocations) ranged from 0.5 (for 200 MeV n^{-1} Fe-56) to 7.8 (for 500 MeV n^{-1} Ar-40). The values found for total (i.e. simple plus complex) exchanges were even higher, due to the significant contribution of complex exchanges. Both for simple and for total exchanges, the RBE values derived from metaphase data were higher than the corresponding PCC values. The RBE–LET relationship, which reached a maximum around 150 keV micron^{-1}, is consistent with other literature studies on CA induction (e.g. Testard *et al* 1997, Wu *et al* 1997). Besides outlining the issue of possible biases due to interphase death/mitotic delay, which can be overcome thanks to the PCC technique, these studies clearly show that for heavy ions the scoring of complex exchanges is a crucial issue. Of course, such a scoring is strongly dependent on the chromosome painting technique utilized. A recent multi-FISH study (each chromosome painted with a different colour with respect to the others) of CA induction in human lymphocytes exposed to 1000 MeV n^{-1} iron ions and treated with chemically induced PCC (Durante *et al* 2002) showed that at 3 Gy, approximately 80% of exchanges are complex, compared with an average of 50% found by George *et al* (2003) with 2 whole-chromosome FISH probes (i.e. two chromosomes were painted with a different colour) in the dose range 0.2–2 Gy.

4.2. CA induction in carbon therapy patients and astronauts

Therapeutic carbon beams represent the major source of human exposure to heavy ions on Earth, since the Earth's atmosphere protects us from most of the heavy-ion cascades emanating from the GCR. Blood is a normal tissue which is unavoidably exposed during radiotherapy, and the yield of CAs in PBL is considered as a reliable estimate of the equivalent whole-body dose (Edwards 1997). Lymphocytes circulate in the blood vessels and are distributed throughout the body, mainly in lymph nodes, spleen, bone marrow, thymus and the gut lymphoid tissue. Damage to the haematopoietic tissue is therefore a major limiting factor with respect to the total dose delivered in a radiotherapy treatment, both for acute morbidity and for the risk of developing secondary cancers (Kolb 1991). Durante *et al* (2000) monitored the induction of CAs in PBL of cancer patients exposed to a 290 or 350 MeV n^{-1} SOBP at NIRS in Japan, as well as of other patients exposed to 10 MV x-rays. For the 290 MeV n^{-1} carbon beam, the LET was about 13 keV micron^{-1} in the plateau and increased from about 40 keV micron^{-1} in the proximal edge to 200 keV micron^{-1} at the distal fall-off, with clonogenic inactivation RBE values ranging between 2 and 3 along the SOBP. Similar values were found to hold for the 350 MeV n^{-1} beam. Reciprocal exchanges (i.e. dicentrics plus translocations) were the most frequent aberration type scored during radiotherapy, but deletions and complex exchanges were observed as well. The fraction of aberrant PBL was found to increase with the number of delivered dose fractions,

reaching a plateau at high doses. Interestingly, while C-ions were found to be more efficient than x-rays at inducing CAs in PBL *in vitro* (showing a RBE of 1.43 ± 0.17 at 13 keV micron^{-1} and of 3.9 ± 0.4 at 83 keV micron^{-1}), for the patients considered in this study the fraction of aberrant PBL was lower after carbon-ion treatments than after dose equivalent x-ray treatments. This result was interpreted as a proof of the improved dose distribution achieved with C-ions. Furthermore, the fraction of aberrant PBL was found to be well correlated with the lymphocyte loss during the treatment, suggesting that the reduced yield of C-ion-induced aberrations in lymphocytes implies a lower risk of acute bone marrow toxicity with respect to x-rays, as well as a lower risk of secondary cancers (the latter due to the correlation between aberrations in PBL and late cancer incidence, see e.g. Rabbits 1994).

Monitoring of CAs in astronauts' PBL provides an example of CA induction following *in vivo* exposure to space radiation that is a mixed field consisting of high-energy particles including heavy ions. The literature provides many studies (Durante 1996, Fedorenko *et al* 2001, George *et al* 2001a, Obe *et al* 1997, Testard *et al* 1996, Yang *et al* 1997), which taken together show that biodosimetry estimates based on CA measurements lie within the range expected from physical dosimetry. In particular, Durante *et al* (2003) measured CAs in PBL from 33 crew members involved in long-term missions (more than 3 months) on the Mir station or the International Space Station (ISS), as well as short-term taxi flights (less than 3 months), spanning about 10 years (from 1992 to 2003). The average absorbed dose was about 4.3 mGy for short-term flights and 78 mGy for long-term missions. While the dicentric yields observed after short-term missions were not significantly higher with respect to pre-flight control levels, those measured following long-term missions in PBL taken from cosmonauts at their first flight showed a highly significant increase, consistent with the values calculated from physical dosimetry data. The maximum post-flight dicentric yield (0.0075 ± 0.0028 dicentrics cell^{-1}) was observed for an astronaut who made a spaceflight of 189 days, receiving 81 mGy. Comparison of post-flight dicentric yields with pre-flight gamma-ray calibration curves indicated that the observed increase of dicentrics after long-term missions would correspond to an equivalent dose of 0.2 Sv, corresponding to a low-Earth-orbit space radiation quality factor of about 2.5. This is consistent with the value of 2.4 calculated by Badhwar *et al* (2002). Interestingly, for cosmonauts involved in two or more space flights, the frequencies of dicentrics and translocations declined rapidly between two subsequent spaceflights, and the yields of stable translocations at the end of the last mission were generally of the same order as background aberration frequencies measured before the first mission. This might be explained by taking into account changes in the immune system (and thus lymphocyte survival and repopulation) under microgravity conditions and/or other phenomena such as adaptive response to space radiation.

4.3. A theoretical model of CA induction based on radiation track structure

Despite the recent significant advances in the experimental techniques and the large amount of available data, some aspects of the mechanisms governing the induction of CAs have not been fully elucidated yet. For instance, it is still not clear whether any single DNA DSB, independent of its complexity, can participate in the formation of CAs, or if only severe (i.e. clustered) breaks are involved. Furthermore, while it is widely recognized that only DNA breaks sufficiently close in space can interact and form exchange-type CAs, the relationship linking the distance between the two breaks and their interaction probability is still not known. Theoretical models

and simulation codes can be of great help both for elucidating the mechanisms underlying experimental observations and for performing extrapolations where the experimental data are not available, typically at low doses and/or low dose rates. Various modelling approaches can be found in the literature, and many of them are based on Lea's 'breakage-and-reunion' theory (Lea 1946). According to Lea, the radiation can induce chromosome breaks, and each break produces two independent chromosome free ends. Those free ends that are sufficiently close can interact and give rise to exchanges via pair-wise 'mis-rejoining'. Though Revell's 'Exchange theory', which is based on the interaction between pairs of chromosome breaks (*not* break free-ends), was applied by various authors, the models based on Lea's approach better describe the induction of complex exchanges. Various reviews on the CA induction theories and models are available in the literature (e.g. Edwards 2002, Hlatky *et al* 2002, Ottolenghi *et al* 1999, Savage 1998). In the following, we will present one of the few modelling approaches that can deal with heavy ions, since the majority of the available literature is limited to photons and/or light ions.

In 1999, Ballarini *et al* (1999) developed an *ab initio* mechanistic model and a Monte Carlo code based on radiation track structure at the nanometre level. The current version of the model can simulate the induction of the main CA types (including dicentrics, translocations, rings, various complex exchanges and deletions) in human cells—typically lymphocytes—exposed to photons, light ions—typically protons and alpha particles—and heavy ions such as carbon and iron (Ballarini and Ottolenghi 2003, 2004, 2005, Ballarini *et al* 2002, 2006, 2007).

The main assumption of the model consists of regarding CAs as the 'evolution' of clustered, and thus severe, DNA breaks, called 'complex lesions' (CLs). On the basis of Lea's theory, each CL is assumed to produce two independent chromosome free ends. Only free ends induced in neighbouring chromosomes or in the same chromosome are allowed to join and give rise to exchange-type aberrations, reflecting the experimental evidence that DNA repair takes place within the channels separating the various chromosome 'territories'. The latter are basically non-overlapping intra-nuclear regions occupied by a single chromosome during interphase. The current version of the model mainly deals with human lymphocyte nuclei, which are modelled as 3-micron radius spheres. The implementation of human fibroblast cell nuclei, which as a first approach are described as thin cylinders, is in progress. Both for lymphocytes and for fibroblasts, the 46 chromosome territories are described as (irregular) intra-nuclear domains with volume proportional to the chromosome DNA content, and each territory consists of the union of small adjacent cubic boxes. Repetition of chromosome territory construction with different chromosome positions provides different configurations for lymphocyte nuclei in the G_0 phase of the cell cycle.

The yield of induced CL Gy^{-1} $cell^{-1}$, taken from track-structure simulations provided by the PARTRAC code mentioned above, is the starting point for dose–response-curve simulations. While for photons the lesions are randomly distributed in the cell nucleus, for light ions they are located along straight lines representing traversals of cell nuclei. Concerning heavy ions, a fraction of the lesions induced by a heavy ion are 'shifted' radially to take into account the effects of delta rays. Specific background (i.e. prior to irradiation) yields for different aberration types can be included. Both Giemsa staining and whole-chromosome FISH painting can be simulated, and the implementation of multi-FISH is in progress. Repetition of the process for different dose values provides dose–response curves for the main aberration types, directly comparable with experimental data. Further details on the simulation methods can be found elsewhere (e.g. Ballarini *et al* 2007). A representation of the two available cell nucleus target models is shown in figure 4.

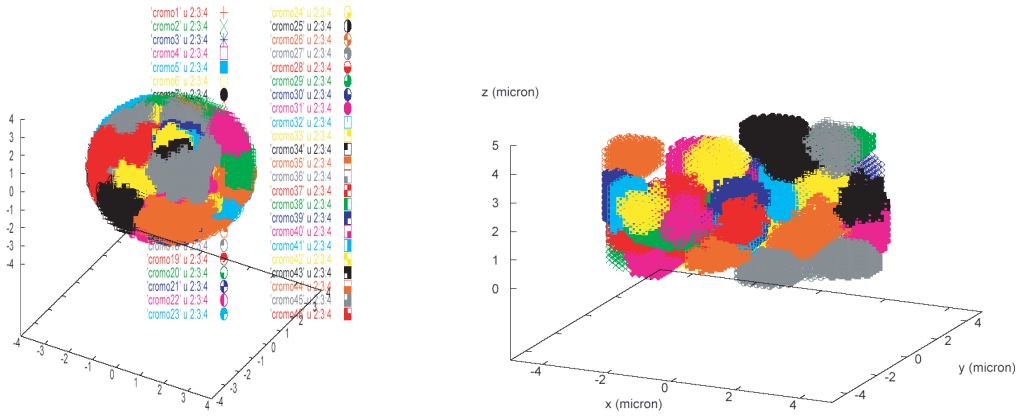

Figure 4. Available cell nucleus target models (left panel: lymphocyte nucleus; right panel: fibroblast nucleus) with the 46 chromosome territories represented in different colours.

Table 1. Predicted and observed whole-genome simple chromosome exchanges (dicentrics plus reciprocal translocations) per 100 cells induced in human lymphocytes exposed to different doses of 290 MeV n^{-1} carbon ions and 1 GeV n^{-1} Fe ions (nominal energies). The experimental data reported for comparison, obtained using whole-chromosome FISH probes associated with chemically induced PCC, were taken from George *et al* (2003).

Ion type	Dose (Gy)	Model prediction	PCC data
C	0.1	3.7	4.8 ± 0.8
C	1.2	65.6	60.1 ± 0.8
Fe	0.2	13.2	16.6 ± 2.5
Fe	0.5	31.1	46.5 ± 6.0
Fe	1.0	64.4	76.3 ± 12.9
Fe	1.5	94.4	94.5 ± 18.2
Fe	2.0	115.6	114.3 ± 19.9

In previous works, the model has been tested for gamma rays, protons and He ions by comparing the simulated dose–response curves with the experimental data available in the literature, without performing any fit *a posteriori.* The good agreement between the model predictions and experimental data for the induction of different aberration types allowed for the model validation. Furthermore, the model has been applied to the evaluation of chronic myeloid leukaemia (Ballarini and Ottolenghi 2004), which is thought to arise from a reciprocal translocation involving chromosomes 9 and 22, and to the estimation of dicentric yields in astronauts' lymphocytes following long-term missions onboard the Mir space station and the ISS (Ballarini and Ottolenghi 2005). The extension of the model to heavy ions has started only recently, and the results are still preliminary. An example is reported in table 1, which shows calculated yields (average number per 100 cells) of whole-genome simple exchanges (i.e. dicentrics plus reciprocal translocations) induced by 290 MeV n^{-1} carbon ions (LET = 13.3 keV micron^{-1}) and 1 GeV n^{-1} Fe ions (LET = 147 keV micron^{-1}). The experimental data taken from the literature (George *et al* 2003) are also reported for comparison.

In the framework of space radiation research, which deals with low doses and thus low fluences down to single traversals of the cell nucleus, we calculated that a single traversal by a 1 GeV n^{-1} H ion (or even a He-ion) does not give rise to aberration yields higher than typical background levels of unirradiated controls ($\sim$0.001 dicentrics $cell^{-1}$and 0.005 translocations $cell^{-1}$). On the contrary, a single traversal by a 1 GeV n^{-1} iron ion, which has higher charge and thus higher LET, was found to induce 0.26 dicentrics (and 0.26 reciprocal translocations) per cell, and 0.45 complex exchanges per cell. In this context, we calculated that a lymphocyte nucleus (represented as a 3-μm radius sphere) traversed by exactly one 1 GeV proton receives a dose of about 0.0012 Gy, whereas the same nucleus traversed by exactly one 1 GeV n^{-1} Fe ion receives a dose of about 0.83 Gy. These findings reflect the role played by LET in modulating the radiation effects.

5. Conclusions

In this paper, we have discussed the main physical features of heavy-ion track structure, including inelastic scattering cross-sections in liquid water. More specifically, we have derived the general non-relativistic quantum mechanical expression of the single and double differential cross sections, which can then be related to the dielectric properties of the medium (e.g. Landau 1984, Pines and Nozieres 1966). The extension of the general quantum mechanical expression of the inelastic scattering cross section expressed in terms of the dielectric properties of the medium, allows one to take into account different mechanisms, such as polarization effects of the medium following charged particle traversal, which can give different contributions to the calculation of energy loss in condensed media such as liquid water. Examples of ion tracks simulated by means of the PARTRAC code were also shown, outlining the differences between light ions and heavy ions such as carbon (which is of interest for hadron therapy) and iron (which is of interest for space research). This allowed quantification of the different levels of energy-deposition clustering which characterize ions having the same velocity (that is, the same energy per nucleon) but different charge, and thus different LET. Heavy-ion tracks are much more clustered than light-ion tracks (especially protons) due to the higher charge and LET and shorter MFP. Since the radiation track structure at the nanometre level can modulate the effects in biological targets, we focused on heavy-ion induced DNA DSBs and CAs. The analysis (again performed by means of the PARTRAC code) of the induction of DNA fragments in human cells irradiated with 115 MeV n^{-1} iron ions allowed quantification of DSB spatial correlation. More specifically, such ions were found to be particularly effective at inducing fragments smaller than 1 kbp, which account for about half of the total fragments, although they can hardly be detected in experiments. To further investigate the role played by radiation quality in modulating DNA fragmentation, in the future we intend to extend the work to different energies.

Concerning CAs, after discussing CA induction by heavy ions both *in vitro* and *in vivo* (i.e. in cancer patients treated with carbon ions and in astronauts exposed to space radiation), we presented a model and a Monte Carlo code which started being developed in our group several years ago. The model, which is based on the assumption that only clustered DNA breaks can give rise to aberrations, is now able to deal not only with photons and light ions, but also with heavy ions such as carbon and iron. The results obtained to date confirm the fundamental role of DNA-break clustering, as well as peculiar features of heavy ions such as the effective induction of complex exchanges and of interphase death/mitotic delay. As a natural evolution of this work, in the future we intend to extend our model to other cell types, typically fibroblasts. Moreover,

further studies are desirable on the relationships between CAs and cell clonogenic inactivation. Indeed, it is well known that the specific aberration types (e.g. dicentrics and some complex exchanges) imply a lower probability for the cell to survive mitosis, whereas other aberrations (e.g. reciprocal translocations) are generally transmitted to the cell progeny.

Overall, the analysis presented in this paper provided a quantification of the role played by heavy-ion track structure in modulating the induction of important radiobiological damage such as DNA DSBs and CAs.

Acknowledgments

This work was partially supported by the EU ('RISC-RAD' project, contract no FI6R-CT-2003-508842, and 'NOTE' project, contract no FI6R-036465) and ASI (Italian Space Agency, 'Mo-Ma/COUNT' project).

References

Alloni D, Ballarini F, Belli M, Campa A, Esposito G, Friedland W, Liotta M, Ottolenghi A and Paretzke H 2007 Modeling of DNA fragmentation induced in human fibroblasts by ^{56}Fe ions *Adv. Space Res.* **40** 1401–7

Alloni D 2008 Radiation biophysics modelling: track structure theoretical bases and Monte Carlo simulations of DNA damage *PhD Thesis* University of Pavia, Italy

Amaldi U and Kraft G 2007 European developments in radiotherapy with beams of large radiobiological effectiveness *J. Radiat. Res.* **48** (Suppl. A) A27–41

Badhwar G, Atwell W, Reitz G, Beaujean R and Heinrich W 2002 Radiation measurements on the Mir orbital station *Radiat. Meas.* **35** 393–422

Ballarini F and Ottolenghi A 2003 Chromosome aberrations as biomarkers of radiation exposure: modelling basic mechanisms *Adv. Space Res.* **31** 1557–68

Ballarini F and Ottolenghi A 2004 A model of chromosome aberration induction and CML incidence at low doses *Radiat. Environ. Biophys.* **43** 165–71

Ballarini F and Ottolenghi A 2005 A model of chromosome aberration induction: applications to space research *Radiat. Res.* **164** 567–70

Ballarini F, Merzagora M, Monforti F, Durante M, Gialanella G, Grossi G, Pugliese M and Ottolenghi A 1999 Chromosome aberrations induced by light ions: Monte Carlo simulations based on a mechanistic model *Int. J. Radiat. Biol.* **75** 35–46

Ballarini F, Biaggi M and Ottolenghi A 2002 Nuclear architecture and radiation-induced chromosome aberrations: models and simulations *Radiat. Prot. Dosim.* **99** 175–82

Ballarini F *et al* 2006 Physics to understand biology: Monte Carlo approaches to investigate space radiation doses and their effects on DNA and chromosomes *Proc. 11th Int. Conf. On Nuclear Reaction Mechanisms, Varenna, Italy, 12–16 June 2006* ed E Gadioli *Ric. Sci. Educ. Permanente Suppl.* **26** 591–600

Ballarini F, Alloni D, Facoetti A, Mairani A, Nano R and Ottolenghi A 2007 Radiation risk estimation: modelling approaches for 'targeted' and 'non-targeted' effects *Adv. Space Res.* **40** 1392–1400

Belli M *et al* 2002 DNA fragmentation in V79 cells irradiated with light ions as measured by PFGE. I. Experimental results *Int. J. Radiat. Biol.* **78** 475–82

Campa A *et al* 2005 DNA DSB induced in human cells by charged particles and gamma rays: experimental results and theoretical approaches *Int. J. Radiat. Biol.* **81** 841–54

Campa A *et al* 2004 DNA fragmentation in V79 cells irradiated with light ions as measured by pulsed-field gel electrophoresis. II. Simulation with a generalized broken stick model *Int. J. Radiat. Biol.* **80** 229–38

Chatterjee A and Schaefer H J 1976 Microdosimetric structure of heavy ion tracks in tissue *Radiat. Environ. Biophys.* **13** 215–27

Dingfelder M *et al* 1998 Electron inelastic-scattering cross sections in liquid water *Radiat. Phys. Chem.* **53** 1–8
Dingfelder *et al* 2000 Inelastic-collision cross sections of liquid water for interaction of energetic protons *Radiat. Phys. Chem.* **59** 255–75
Durante M 1996 Biological dosimetry in astronauts *Riv. Nuovo Cimento* **19** 1–44
Durante M, George K and Yang T 1997 Biodosimetry of ionizing radiation by selective painting of prematurely condensed chromosomes in human lymphocytes *Radiat. Res.* **148** S45–50
Durante M, Furusawa Y, George K, Gialanella G, Greco O, Grossi G, Matsufuji N, Pugliese M and Yang T 1998 Rejoining and misrejoining of radiation-induced chromatin breaks IV charged particles *Radiat. Res.* **149** 446–54
Durante M, Furusawa Y, Majima H, Kawata T and Gotoh E 1999 Association between G2-phase block and repair of radiation-induced chromosome fragments in human lymphocytes *Radiat. Res.* **151** 670–76
Durante M *et al* 2000 X-rays vs carbon-ion tumor therapy: cytogenetic damage in lymphocytes *Int. J. Radiat. Oncol. Biol. Phys.* **47** 793–98
Durante M, George K, Wu H and Cucinotta F 2002 Karyotypes of human lymphocytes exposed to high-energy iron ions *Radiat. Res.* **158** 581–90
Durante M *et al* 2003 Chromosome aberration dosimetry in cosmonauts after single or multiple space flights *Cytogenet. Genome Res.* **103** 40–6
Edwards A 1997 The use of chromosomal aberrations in human lymphocytes for biological dosimetry *Radiat. Res.* **148** 39–44
Edwards A 2002 Modelling radiation-induced chromosome aberrations *Int. J. Radiat. Biol.* **78** 551–8
Ehrenreich H and Cohen M H 1959 Self-consistent field approach to the many-electron problem *Phys. Rev.* **115** 786–90
Fedorenko B *et al* 2001 Cytogenetic studies of blood lymphocytes from cosmonauts after long-term space flights on Mir station *Adv. Space Res.* **27** 355–9
Frankenberg D *et al* 1999 Induction of DNA double-strand breaks by and ions in primary human skin fibroblasts in the LET range of 8 to 124 keV/micron *Radiat. Res.* **151** 540–9
Friedland W, Jacob P, Paretzke H G and Stork T 1998 Monte Carlo simulation of the production of short DNA fragments by low-linear energy transfer radiation using higher-order DNA models *Radiat. Res.* **150** 170–82
Friedland W *et al* 2003 Simulation of DNA damage after proton irradiation *Radiat. Res.* **159** 401–10
Friedland W, Paretzke H G, Ballarini F, Ottolenghi A, Kreth G and Cremer C 2008 First steps towards systems radiation biology studies concerned with DNA and chromosome structure within living cells *Radiat. Environ. Biophys.* **47** 49–61
George K, Durante M, Wu H, Willingham V, Badhwar G and Cucinotta F 2001a Chromosome aberrations in the blood lymphocytes of astronauts after space flight *Radiat. Res.* **156** 731–8
George K, Wu H, Willingham V, Furusawa Y, Kawata T and Cucinotta F 2001b High- and low-LET induced chromosome damage in human lymphocytes: a time course of aberrations in metaphase and interphase *Int. J. Radiat. Biol.* **77** 175–83
George K, Durante M, Willingham V, Wu H, Yang T and Cucinotta F 2003 Biological effectiveness of accelerated particles for the induction of chromosome damage measured in metaphase and interphase human lymphocytes *Radiat. Res.* **160** 425–35
Goodhead D T 1994 Initial events in the cellular effects of ionising radiation: clustered damage in DNA *Int. J. Radiat. Biol.* **65** 7–17
Goodwin E, Blakely E and Tobias C 1994 Chromosomal damage and repair in G1-phase Chinese hamster ovary cells exposed to charged-particle beams *Radiat. Res.* **138** 343–51
Gudowska-Nowak E, Kleczkowski A, Nasonova E, Scholz M and Ritter S 2005 Correlation between mitotic delay and aberration burden, and their role for the analysis of chromosomal damage *Int. J. Radiat. Biol.* **81** 23–32
Heidin L and Lundqvist S 1969 Effects on electron–electron and electron–phonon interactions in the one-electron states of solids *Solid State Phys.* **23** 1–181

Hlatky L, Sachs R, Vazquez M and Cornforth M 2002 Radiation-induced chromosome aberrations: insights gained from biophysical modelling *Bioessays* **24** 714–23

Höglund E, Blomquist E, Carlsson J and Stenerlöw B 2000 DNA damage induced by radiation of different linear energy transfer: initial fragmentation *Int. J. Radiat. Biol.* **76** 539–47

Holley W R and Chatterjee A 1996 Clusters of DNA damage induced by ionizing radiation: formation of short DNA fragments. I. Theoretical modeling *Radiat. Res.* **145** 188–99

Kawata T, Durante M, Furusawa Y, George K, Takai N, Wu H and Cucinotta F 2001 Dose-response of initial G2-chromatid breaks induced in normal human fibroblasts by heavy ions *Int. J. Radiat. Biol.* **77** 165–74

Kolb H 1991 Bone marrow morbidity of radiotherapy *Complication of Cancer Management* ed P Plowman, T McElwain and A Meadows (Oxford: Oxford University) pp 398–410

Landau L D 1984 *Electrodynamics of Continuous Media* (Oxford: Elsevier)

Lea D E 1946 *Actions of Radiations on Living Cells* (Cambridge: Cambridge University Press)

Liotta M 2005 Effetti della struttura di traccia sulle distribuzioni radiali di dose e di Danni al DNA indotti da particelle cariche di interesse in adroterapia '*Laurea*' *Thesis* University of Pavia, Italy

Löbrich M, Cooper P K and Rydberg B 1996 Non-random distribution of DNA double-strand breaks induced by particle irradiation *Int. J. Radiat. Biol.* **70** 493–503

Nasonova E and Ritter S 2004 Cytogenetic effects of densely ionising radiation in lymphoytes: impact of cell cycle delays *Cytogenet. Genome Res.* **104** 216–20

Newman H C, Prise K M, Folkard M and Michael B D 1997 DNA double-strand break distributions in X-ray and alpha-particle irradiated V79 cells: evidence for non-random breakage *Int. J. Radiat. Biol.* **71** 347–63

Obe G, Johannes I, Johannes C, Hallman K, Reiz G and Facius R 1997 Chromosomal aberrations in blood lymphocytes of astronauts after long-term space flights *Int. J. Radiat. Biol.* **72** 727–34

Ohara H, Okazaki N, Monobe M, Watanabe S, Kanayama M and Minamihisamastu M 1998 Induction of asymmetrical type chromosome aberrations in cultures human lymphocytes by ion beams of different energies at varying LET from HIMAC and RRC *Adv. Space Res.* **22** 1673–82

Ottolenghi A, Ballarini F and Merzagora M 1999 Modelling radiation induced biological lesions: from initial energy depositions to chromosome aberrations *Radiat. Environ. Biophys.* **38** 1–13

Pines D and Nozieres P 1966 *The Theory of Quantum Liquids* (New York: Benjamin)

Rabbits T 1994 Chromosomal translocations in human cancer *Nature* **372** 143–9

Ritchie H R *et al* 1988 Physical aspects of charged particle structure *Nucl. Tracks Radiat. Meas.* **16** 141–58

Ritter S, Nasonova E, Furusawa Y and Anduo K 2002 Relationship between aberration yield and mitotic delay in human lymphocytes exposed to 200 MeV/ Fe-ions or x-rays *J. Radiat. Res.* **43** S175–9

Rydberg B 1996 Clusters of DNA damage induced by ionizing radiation: formation of short DNA fragments. II. Experimental detection *Radiat. Res.* **145** 200–9

Rydberg B, Holley W R, Mian I S and Chatterjee A 1998 Chromatin conformation in living cells: support for a zig-zag model of the 30 nanometer chromatin fiber. *J. Mol. Biol.* **284** 71–84

Savage J 1998 A brief survey of aberration origin theories *Mutat. Res.* **404** 139–47

Testard I, Ricoul M, Hoffschir F, Flury-Herard A, Dutrillaux B, Fedorenko B, Gerasimenko V and Sabatier L 1996 Radiation-induced chromosome damage in astronauts' lymphocytes *Int. J. Radiat. Biol.* **70** 403–11

Testard I, Dutrillaux B and Sabatier L 1997 Chromosomal aberrations induced in human lymphocytes by high-LET irradiation *Int. J. Radiat. Biol.* **72** 423–33

Wu H, Durante M, George K and Yang T 1997 Induction of chromosome aberrations in human cells by charged particles *Radiat. Res.* **148** S102–7

Yang T, George K, Johnson A S, Durante M and Fedorenko B 1997 Biodosimetry results from space flight MIR-18 *Radiat. Res.* **148** S17–23

Zaider M *et al* 1990 Towards *ab initio* evaluation of the wave vector and frequency dependent dielectric response function for crystalline water *Radiat. Prot. Dosim.* **31** 23–8